Burns & Trauma, 2023, 11, tkac048
https://doi.org/10.1093/burnst/tkac048
Research Article

OXFORD

Research Article

Zn^{2+}-Loaded adhesive bacterial cellulose hydrogel with angiogenic and antibacterial abilities for accelerating wound healing

Zhengzhe Han[1], Lili Deng[2], Shiyan Chen[2,*], Huaping Wang[2,*] and Yinjun Huang[3,*]

[1]Department of Orthopedic Surgery, and Shanghai Institute of Microsurgery on Extremities, Shanghai Sixth People's Hospital, 600 Yishan Road, Shanghai 200233, P.R. China, [2]State Key Laboratory for Modification of Chemical Fibers and Polymer Materials, College of Materials Science and Engineering, Donghua University, Shanghai 201620, P.R. China and [3]Department of Trauma Center, Shanghai General Hospital, Shanghai Jiao Tong University School of Medicine, Shanghai, 201600, P.R. China

*Correspondence Shiyan Chen, Email: chensy@dhu.edu.cn; Huaping Wang, Email: wanghp@dhu.edu.cn; Yinjun Huang, Email: 972464253@qq.com

Received 26 April 2022; Revised 9 June 2022; Editorial decision 20 October 2022

Abstract

Background: Wound healing is a process that requires angiogenesis and antibacterial activities and it remains a challenge for both experimental and clinical research worldwide. Zn^{2+} has been reported to be widely involved in angiogenesis and exerts antibacterial effects, making it suitable as a treatment to promote wound healing. Therefore Zn^{2+}-loaded adhesive bacterial cellulose hydrogel was designed to observe its angiogenic and antibacterial abilities in the wound healing process.

Methods: The characterization, tensile strength, swelling behaviors and antibacterial activity of bacterial cellulose/polydopamine/zeolitic imidazolate framework-8 (BC/PDA/ZIF8) hydrogels were tested. Cell-Counting-Kit-8 (CCK8), transwell, tube formation and real time qunantitative PCR (qRT-PCR) assays were performed to evaluate the cell compatibility of BC/PDA/ZIF8 hydrogels *in vitro*. A full-thickness defect wound model and histological assays were used to evaluate the BC/PDA/ZIF8 hydrogels *in vivo*.

Results: The prepared BC/PDA/ZIF8 hydrogels exhibited suitable mechanical strength, excellent swelling properties, good tissue adhesion, efficient angiogenic and antibacterial effects and good performance as a physical barrier. *In vivo* experiments showed that the BC/PDA/ZIF8 hydrogels accelerated wound healing in a full-thickness defect wound model by stimulating angiogenesis.

Conclusions: This study proved that BC/PDA/ZIF8 hydrogels possess great potential for promoting satisfactory wound healing in full-thickness wound defects through antibacterial effects and improved cell proliferation, tissue formation, remodeling and re-epithelialization.

Highlights

- Zn^{2+} was loaded into a natural extracellular matrix structure for a stable release to accelerate wound healing. The prepared BC/PDA/ZIF8 hydrogels exhibited multiple advantages, including suitable mechanical strength, excellent swelling properties, good tissue adhesion, efficient angiogenic and antibacterial effects and good performance as a physical barrier.
- BC/PDA/ZIF8 hydrogels could enhance the proliferation, migration and tube formation of endothelial cells.

© The Author(s) 2023. Published by Oxford University Press.
This is an Open Access article distributed under the terms of the Creative Commons Attribution Non-Commercial License (http://creativecommons.org/licenses/by-nc/4.0/), which permits non-commercial re-use, distribution, and reproduction in any medium, provided the original work is properly cited. For commercial re-use, please contact journals.permissions@oup.com

- BC/PDA/ZIF8 hydrogels possess the potential for promoting satisfactory wound healing in full-thickness wound defects.

Key words: Hydrogel, Mechanical properties, Biocompatibility, Angiogenic effects, Wound healing

Background

The skin is the largest organ and the first barrier of the human body [1]. It protects the organism from various kinds of injuries, such as mechanical injuries, infections and severe temperatures, but can be damaged itself in the process [2]. Wound defects cost billions of dollars every year worldwide, imposing a socioeconomic burden on all human beings [3]. The basic therapy to treat wound defects is still wound dressing [4]. An adequate wound dressing may accelerate wound healing progress and reduce morbidity and the financial burden suffered by patients. Ideal wound dressings should possess moisturizing properties, exhibit satisfactory mechanical performance, promote wound healing, absorb exudate, exert antibacterial effects and have other beneficial characteristics [5]. To date, various kinds of wound dressings based on biomaterials have been developed and applied widely to healing wounds, including foam, electrospun nanofibers, aerogels, sponge-modified gauze and hydrogels [6]. Among such materials, hydrogels are promising for use in wound dressing and are widely applied to treat wounds under many conditions. Hydrogels play an essential role in maintaining the moist environment of wound defects and act as a physical barrier against mechanical injuries [7].

Bacterial cellulose (BC) is a promising biomaterial due to its remarkable inherent properties, such as suitable mechanical performance, good water retention, high porosity and attractive biocompatibility [8]. In addition, the 3D network structure, formed by loose nanofibrils, promotes cell adhesion and nanoparticle insertion. Luo *et al*. [9] discussed a flexible BC dressing synthesized containing ZnO, which possessed desirable antibacterial properties, whereas ZnO accumulation alone showed drastic cytotoxicity. As an ideal wound dressing material, BC hydrogel was also used for chronic wound dressings in the work of Daria and co-workers, who modified BC to improve its absorption ability after drying; however, BC alone is insufficient for a complicated wound whose healing process must be promoted. [10] It has been proven that Zn^{2+} can stimulate angiogenesis and inhibit the growth of *Escherichia coli* (*E. coli*) and *Staphylococcus aureus* (*(S. aureus)*), thereby promoting wound healing. Slow and sustained Zn^{2+} release is extremely important in wound dressings, as excessive Zn^{2+} may cause adverse effects on cell proliferation. The covalent bonding of Zn^{2+} and dimethylimidazole in the synthesis of zeolitic imidazolate framework-8 (ZIF8) can enable effective long-term release.

Herein, a multifunctional hydrogel based on natural extracellular matrix (ECM) hydrogels with long-term stable Zn^{2+} release was designed and found to exhibit outstanding angiogenesis and antibacterial properties for promoting wound healing. Polydopamine (PDA) was used to induce the *in situ* growth of ZIF8 in the BC porous structure (Figure 1). This approach not only deposits nanoparticles but also prevents agglomeration. The hydrogel's microscopic morphology, mechanical properties and swelling properties were characterized. Furthermore, the biocompatibility of BC/PDA/ZIF8 hydrogels was evaluated by analyzing cell compatibility *in vitro* [11]. An *in vivo* experiment was used to evaluate the effect of multifunctional BC/PDA/ZIF8 hydrogels on the wound healing progress of full-thickness skin tissue defects in rats [12].

Methods

Materials

NaOH was purchased from Sinopharm Chemical Reagent Co. Ltd. 2-Methylimidazole (2-Mim, 99%) was purchased from Shanghai Macklin Biochemical Co., Ltd. Zinc nitrate hexahydrate ($Zn(NO_3)_2{\cdot}6H_2O$, 99%) was purchased from Shanghai Titan Scientific Co. Ltd (Shanghai, China). Dopamine hydrochloride (DA) was purchased from Sigma–Aldrich Co., Ltd. Methanol was purchased from Sinopharm Chemical Reagent Co., Ltd (China). All chemicals were used directly without any further purification. All animal experimental procedures were approved by Shanghai Rat & Mouse Biotech Co.,Ltd [IACUC Issue No. 20220928 (11)].

Preparation of BC hydrogels

BC hydrogels (3 mm thickness) were prepared by our team as reported previously [13]. Briefly, BC films were produced by inoculating *Gluconacetobacter xylinus* into basal medium (glucose 5 wt%, yeast extract 0.5 wt%, bacto-peptone 0.5 wt%, disodium phosphate 0.2 wt%, monopotassium phosphate 0.1 wt% and citric acid 0.1 wt%) for 5 days at 30°C in a static culture. Then, the BC was washed several times with deionized water after boiling in 0.1 mol/l NaOH for 1 h to remove impurities (such as dead bacteria and endotoxin) until the pH was neutral. The BC hydrogel was then cut into 4×4 cm wafers and stored at 4°C for further use.

Synthesis of BC/PDA/ZIF8 hydrogels

The hydrogel was synthesized *in situ* by mechanochemical procedures; the synthesis process is shown in Figure 1. The material ratio of ZIF8 was determined as described in the previous literature [14]. Taking BC/PDA/ZIF8–1 as an example, $Zn(NO_3)_2{\cdot}6H_2O$ (0.059 g) and 2-Mim (0.13 g) were dissolved in 5 and 20 ml of deionized water, respectively, to form

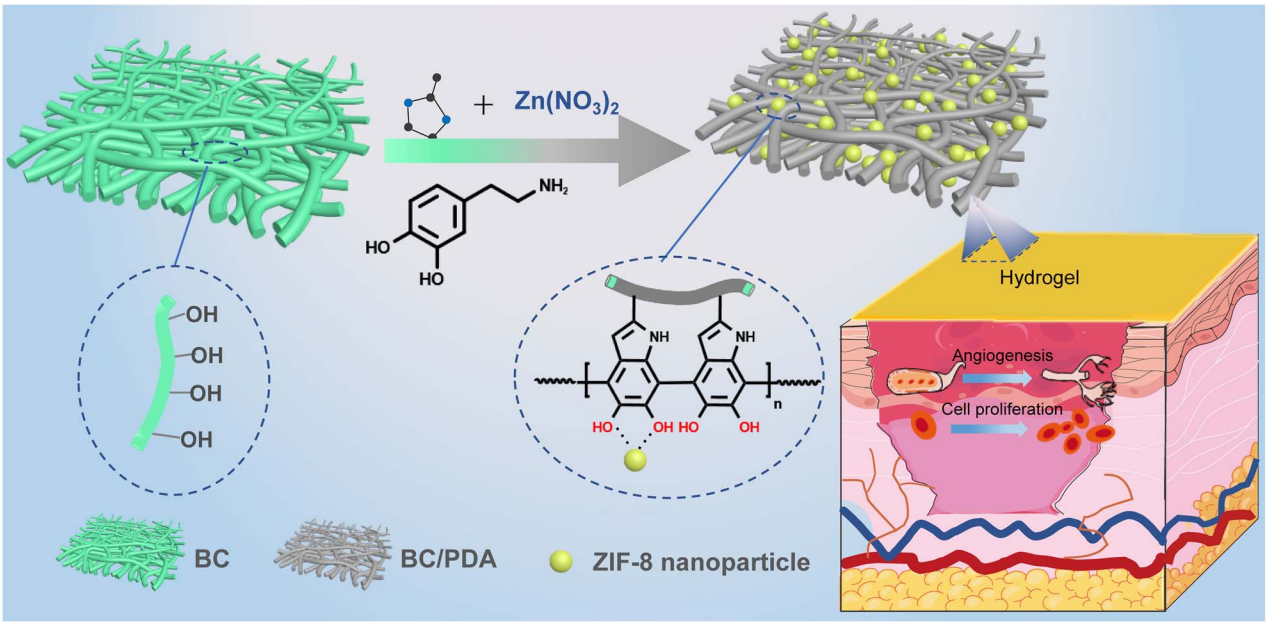

Figure 1. Preparation of BC/PDA/ZIF8 hydrogels. *BC* bacterial Cellulose, *PDA* polydopamine, *ZIF8* zeolitic imidazolate framework 8

a homogeneous solution. Then, DA (0.095 g, 0.02 M) was added to $Zn(NO_3)_2$ solution with stirring to form solution A. After that, solution A was added to the 2-Mim solution in an agate vessel, which was placed in a planetary mill machine for mechanical grinding at a speed of 400 rpm for 20 min. The hydrogels were fabricated by immersing a pressed BC wafer into the above milling solution and moving it to a glass container with constant shaking at 160 rpm for 24 h at 30°C. Finally, the BC/PDA/ZIF8 hydrogels were rinsed with a large amount of deionized water to remove the residual chemicals. BC/PDA/ZIF8–2, BC/PDA/ZIF8–3 and BC/PDA/ZIF8–4 were synthesized from $Zn(NO_3)_2{\cdot}6H_2O$ (0.118 g) and 2-Mim (0.26 g), $Zn(NO_3)_2{\cdot}6H_2O$ (0.177 g) and 2-Mim (0.39 g), $Zn(NO_3)_2{\cdot}6H_2O$ (0.177 g) and 2-Mim (0.42 g), respectively. The other steps were the same as those for BC/PDA/ZIF8–1. For BC/PDA, DA (0.095 g, 0.02 M) was added to 25 ml of deionized water to form a homogeneous solution, which was adjusted to pH 8.5 with Tris aqueous solution. Then, BC hydrogel was added and the mixture was transferred to a constant temperature shock box at 160 rpm for 24 h at 30°C.

Characterization of BC and BC hydrogels

Fourier transform infrared (FTIR) spectra were recorded on an FTIR NEXUS-670 spectrometer over a scan range of 4000–500 cm^{-1}, with a resolution of 2 cm^{-1}. Morphological analysis of the hydrogels was performed by S-4800 field emission scanning electron microscopy. Samples for observation were freeze-dried for 48 h and sputter-coated with gold. Powder X-ray diffraction (XRD) measurements were performed by a Rigaku D/MAX-2550PC X-ray diffractometer with Cu Kα irradiation from 5–90°. A tensile strength test was carried out under ambient conditions on a universal material testing machine (Instron 5969) equipped with a 100 N load cell at a speed of 20 mm/min. The hydrogels were investigated by an ultraviolet (UV)–visible spectrometer (UV3600, Japan).

Swelling properties

The swelling behaviors of the hydrogels were examined by immersing the freeze-dried BC and BC hydrogels in phosphate-buffered saline (PBS). The weight of the swollen samples was recorded at a predetermined time (0.5, 1, 2, 4, 6, 8, 10, 12 and 24 h) after removal of any excess surface solution by filter paper. Three parallel experiments were carried out for each sample. The swelling ratio of the hydrogel was calculated using the following equation:

$$\text{Swelling ratio } (\%) = \frac{W_s - W_i}{W_i} \times 100$$

where W_i is the weight of the initial freeze-dried sample and W_s is the weight of swollen samples at different time intervals.

In vitro release and antibacterial activity of Zn^{2+}

The release of Zn^{2+} was evaluated by immersing the prepared hydrogels in PBS. Specifically, BC/PDA/ZIF8 hydrogels with different ZIF8 contents were immersed in 30 ml of PBS (pH = 7.4) with constant shaking at 150 rpm at 37°C. Then, 5 ml of the solution was collected at regular time intervals (24, 48, 96h, 4, 5, 6, 7 . . . 14 days) and another 5 ml of fresh PBS was added for replacement. The release content of Zn^{2+} was measured by optical emission spectroscopy (ICP-OES).

The antibacterial activity was evaluated by inhibitory ring and colony forming units (CFU) against *E. coli* and *S. aureus*. For the inhibition ring test, a bacterial solution with a concentration of 10^5 cells/ml was prepared, and 100 ml of the bacterial solution was spread on an agar plate. Then,

a hydrogel sample (ϕ8 mm) was placed on the agar plate. After incubating at 37°C for 24 h, the inhibition ring was observed. For CFU, the sterilized hydrogel was put into the diluted bacterial solution and incubated at 37°C for 24 h. The bacterial solution was diluted and 100 ml was uniformly spread on the agar plate. A photograph was taken and the number of bacterial colonies was counted. The killing rate was calculated by the following formula:

$$\text{Killing rate } (\%) = \frac{N_c - N_e}{N_c} \times 100$$

N_c represents the number of bacteria in the control group (BC) and N_e is that in the experimental group (BC/PDA/ZIF8 hydrogel).

In vitro cytotoxicity

Cells and cell culture The response of fibroblasts and human umbilical vein endothelial cells (HUVECs) to the BC/PDA/ZIF8 hydrogels was studied. The cells were incubated in DMEM supplemented with 10 vol% FBS and 1 wt% penicillin-streptomycin (P/S) with extracts of BC/PDA, BC/PDA/ZIF8–1 and BC/PDA/ZIF8–3 hydrogels at 37°C in a humidified atmosphere containing 5% CO_2. The medium was changed every 3 days. When cell confluence was 90%, the cells were digested with 0.25 wt% trypsin–EDTA and passaged for experiments [15].

Cell proliferation The effect of the BC/PDA/ZIF8 hydrogels on the proliferation of HUVECs and fibroblasts was determined using a cell viability assay Cell-Counting-Kit-8 (CCK8) [16]. In general, cells were seeded on 96-well plates and treated with the extracts of BC/PDA, BC/PDA/ZIF8–1 and BC/PDA/ZIF8–3 hydrogels for 1, 3 and 5 days [17]. The absorbance of the plate was measured at 450 nm with a spectrophotometric microplate reader. The results were expressed as the optical density (OD) of the wells in the plate.

$$\text{Cell viability } (\%) = \frac{OD_{exp} - OD_{blank}}{OD_{exp} - OD_{blank}} \times 100$$

OD_{exp} is the value of BC/PDA/ZIF8–1 and BC/PDA/ZIF8–3 on the given day, and OD_{blank} is the value of BC/PDA.

HUVEC migration and tube formation The effect of the BC/PDA/ZIF8 hydrogels on HUVEC migration was evaluated via a transwell assay [18]. HUVECs (2×10^4) were seeded in the upper chamber of a 24-well transwell plate. Then, 500 μl of extracts of the BC/PDA, BC/PDA/ZIF8–1 and BC/PDA/ZIF8–3 hydrogels were introduced into the lower reservoir. After incubation for 24 h, the top compartments were gently taken and the cells on the upper surface were removed. Cells on the lower surface were fixed with 4% paraformaldehyde for 10 min, stained with 0.5% crystal violet for 10 min and then counted. Three randomly selected fields (200 ×) were taken per compartment [19].

To detect the tube formation activity of the HUVECs, the connected network tubes were allowed to form on Matrigel. Cold Matrigel (500 μl) was placed into a well of a 24-well plate on ice. Then, the Matrigel was covered with HUVEC suspension (5×10^4 cells/well) and the cells were treated with extracts of the BC/PDA, BC/PDA/ZIF8–1 and BC/PDA/ZIF8–3 hydrogels. The tube formation potential was evaluated by counting the tubule number in the network under a microscope (100 ×) after incubation for 6 h [20].

RNA isolation and real time qunantitative PCR (qRT-PCR) analysis Total RNA was extracted from cells with TRIzol reagent (Invitrogen, USA) and quantified with a spectrophotometer (Thermo Scientific, USA). Subsequently, the PrimeScript RT reagent kit (TaKaRa Biotechnology, Japan) was used to perform reverse transcription. Finally, qPCR was conducted on a QuantStudio 6 Flex system (Life Technologies, USA) using the SYBR Green system (Gene Copoeia, USA) to quantify the expression of relevant genes. The relative quantification of target genes was normalized to that of glyceraldehyde-3-phosphate dehydrogenase (GAPDH) and the 2-ΔΔCt method was used to calculate the fold changes [21].

In vivo wound healing

Animals and surgical procedures The effect of the hydrogel on wound healing *in vivo* was evaluated using a full-thickness skin defect model in 18 Sprague–Dawley rats (330–350 g) [22]. The hydrogels were disinfected with UV light prior to implantation. The rats were grown in an specific pathogen free (SPF) environment. Before surgery, anesthesia was administered intraperitoneally with 3% pentobarbital sodium at a dosage of 1.0 ml/kg. Defect ranges were marked, and regulated full-thickness skin wounds (diameter = 2.0 cm) were constructed on the rats by excising the dorsal skin. Then, the wounds were filled with BC/PDA, BC/PDA/ZIF8–1 and BC/PDA/ZIF8–3 hydrogels, respectively. Clean gauze was placed around the wound. Transparent film dressing was applied to the wound to fix the hydrogels in place for the duration of the experiment. After surgery, every rat received an injection of penicillin as an antibiotic. The penicillin was dissolved in normal saline at a concentration of 800 000 U/ml and a dose of 80 000 U per rat [23].

Measurement of wound size reduction Photographs of the rats were taken by a camera on days 0, 3, 7 and 14 post-surgery [24]. The wound margin and range were measured by analysis software (NIH Image). The amount of wound closure was calculated using the following formula:

$$\text{Wound area ratio } (\%) = \frac{A_0 - A_t}{A_0} \times 100$$

where A_0 is the initial wound area ($t = 0$) and A_t is the wound area at each time point.

Histologic, immunohistochemical and immunofluorescence analysis The rats were sacrificed at 7 and 14 days after surgery. The wound tissues with surrounding healthy skin were removed. Formalin was used to fix the samples. Then, the samples were dehydrated and embedded in paraffin. Sections 6 μm thick were stained with hematoxylin–eosin (H&E) and Masson's trichrome [24,25]. These sections were observed under the microscope and new epithelium was determined.

Immunohistochemical and immunofluorescence staining was performed on the sections to determine angiogenesis in wound healing [26]. Immunofluorescence staining was utilized to show platelet endothelial cell adhesion molecule-1 (CD31) (1:100, red color) and alpha-smooth muscle actin (α-SMA) (1:100, green color), which are markers of endothelial cells. Immunohistochemical staining was also performed in our study to show CD31 in samples.

For immunohistochemical staining, the samples were rehydrated and heated for antigen exposure. Then, they were incubated with a primary antibody at 4°C overnight. Next, the secondary antibody was applied and stained with diaminobezidin (DAB). Subsequently, hematoxylin was used for staining. The sections were analyzed by microscopy [26].

For immunofluorescence staining, the slides were rehydrated and blocked with 1.5% goat serum. The primary antibody was incubated at 4°C overnight. The secondary antibody and 4′, 6-diamidino-2-phenylindole (DAPI) were then applied and the slides were analyzed using a fluorescence microscope. The vessels were quantitated for different samples in each group.

Statistical analysis

The data are presented as the mean ± SD. Two-way analysis of variance (ANOVA) and t tests were completed to determine the level of significance and $p < 0.05$ was recognized to be significant. In this research, the most commonly *post hoc* test was used to determine where the differences truly came after a statistical result was found. Statistical comparison in each group was made using GraphPad Prism (GraphPad Prism 9.0, GraphPad Software, USA).

Results

Characterization of BC and BC hydrogels

The experimental design of this study is shown in Figure 1. First, ZIF8 was synthesized with a coating of PDA. After transfer into reagent bottles with BC hydrogel, PDA gradually deposited on the nanofibrils of the BC hydrogel via oxidation and self-polymerization of DA; at the same time, ZIF8 precoated with PDA also deposited and agglomerated on the nanofibrils of the BC hydrogel. The nanocomposites obtained were characterized by FTIR, XRD, tension mechanism and swelling properties, as shown in Figure 2.

As shown in the FTIR spectra in Figure 2a, the spectra of all the hydrogels contained intensity peaks of BC at 3343, 2900, 1050 and 1161 cm^{-1}, which were attributed to O–H, C–H, C–O and C–O–C stretching vibrations, respectively [27]. After modification with PDA, the characteristic band at 1570 cm^{-1} was attributed to the stretching of aromatic C=C bonds of indole (as a typical feature of PDA), providing evidence of successful PDA synthesis in BC [28]. The characteristic peaks of the BC/PDA/ZIF8 hydrogel located at 1570, 1418, and 995 cm^{-1} and 1308 cm^{-1} matched the C=N stretch, C–N stretch and imidazole bending, respectively [29]. This result indicated that ZIF8 was successfully synthesized in BC hydrogels.

Figure 2b shows the XRD spectra of the BC, BC/PDA and BC/PDA/ZIF8 hydrogels. The curve of BC shows the characteristic peaks of its own crystal structure at $2\theta = 14.5$ and 22.5°, corresponding to the crystallographic planes (110) and (200), respectively, which can also be found in BC/PDA and BC/PDA/ZIF8 hydrogels, while PDA did not change the overall structure of cellulose. For the composites, characteristic peaks of ZIF8 between 6 and 20°, including the (011), (002), (112), (013) and (222) planes, are observed clearly [30] and become increasingly obvious with increasing ZIF8 content.

The swelling ratio is an essential performance indicator of the ability of an ideal wound dressing to absorb exudates, which can promote the proliferation of fibroblasts [31]. As shown in Figure 2c, d, although the swelling ratio decreased with increasing ZIF8 content, all the values were >1000%, which suggests a suitable water absorption capacity. Appropriate mechanical strength and good flexibility are also indispensable requirements for ideal wound healing materials [32]. The mechanical properties of the hydrogels were examined by their stress–strain curves and modulus curves, as shown in Figure 2e, f.

Morphology and contact angle of BC and BC composites

We found that the color of the hydrogels turned dark after the *in situ* synthesis of PDA on BC, while the BC hydrogels were transparent (Figure 3a). The macrophotograph shows a uniform black hydrogel (Supplementary Figure S1a, b, see online supplementary material). There was no change in the hydrogel placed in the ultrasonic machine for 1 h. No sediment was found after centrifugation of the ultrasonic solution (Supplementary Figure S1a). The same result was found when the hydrogel was immersed in deionized water for 3 days (Supplementary Figure S1b). The morphology of the BC and BC/PDA/ZIF8 hydrogels was detected by scanning electron microscopy [33,34]. From Figure 3b, the ultrafine 3D network structure of BC and the well-organized nanofibrils with a diameter of 20–80 nm can be seen clearly. The natural ECM offers a satisfactory template for cell proliferation [35]. PDA was mostly coated around the nanofibrils of the BC hydrogel, which made it suitable for inducing the deposition of nanoparticles, and it did not significantly affect the 3D pores of BC in the microstructure of BC/PDA (Figure 3b). As shown in Figure 3b, PDA-coated ZIF8 nanoparticles with a size of ~70 nm (Supplementary Figure S2, see online supplementary

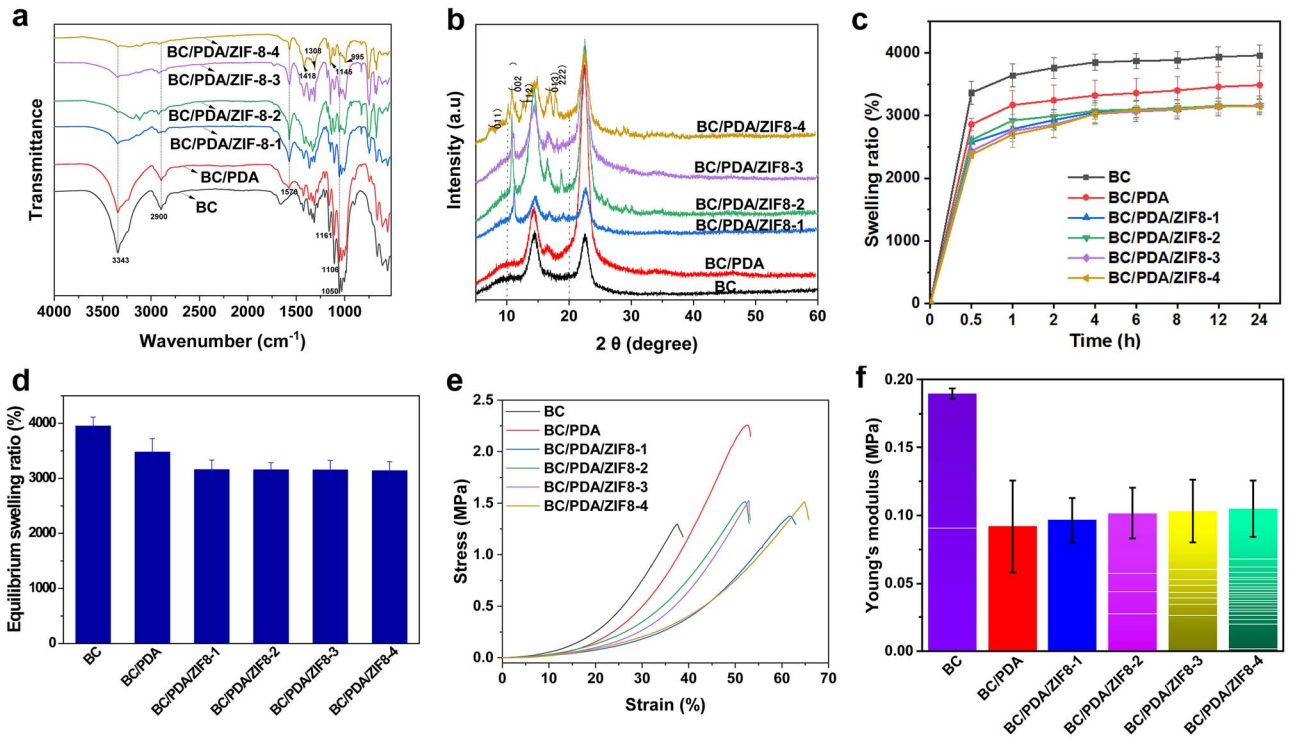

Figure 2. Characterization of BC and BC composite hydrogels. (**a**) FTIR spectra range from 4000–400 cm^{-1}, (**b**) XRD patterns with the 2θ range from 5–60°, (**c**) swelling ratios in 24 h, (**d**) equilibrium swelling ratios, (**e**) stress-strain curves and (**f**) Young's modulus of BC, BC/PDA, BC/PDA/ZIF8 hydrogels. *FTIR* fourier transform infrared spectroscopy, *XRD* X-ray diffraction, *BC* bacterial cellulose, *PDA* polydopamine, *ZIF8* zeolitic imidazolate framework 8

material) were uniformly distributed in the 3D BC structure, especially ZIF8 nanoparticles with low loading [36]. With increasing concentrations of ZIF8, an increasing number of nanoparticles deposited on the nanofibrils. After reaching a certain content, nanoparticles tended to agglomerate to each other in BC/PDA/ZIF8–4 (Figure 3b). The hydrophilicity of the material is a crucial feature for cell adhesion that can be detected by contact angle measurements, as shown in Figure 3c.

Evaluation of the release of Zn^{2+} and antibacterial activity of BC/PDA/ZIF8

As an essential component of various enzymes, Zn^{2+} plays a crucial role in wound healing because it is involved in cell growth and migration in the proliferation and maturation stages [37]. Moreover, the stable and durable release of metal ions is necessary for biomaterials in practical applications [37]. We designed a metal–organic frame (ZIF8) containing Zn^{2+} to prevent abrupt release and investigated the release of Zn^{2+} in PBS at different pH values during wound healing (Figure 4a, b). The amount of Zn^{2+} release from the hydrogels in PBS was proportional to the content of ZIF8 and exhibited a steady upward trend over time. The cumulative release of Zn^{2+} increased with increasing ZIF8 content. Compared to the condition of pH = 7.4 (Figure 4a), hydrogels in an acid environment (Figure 4b) released more Zn^{2+} in 14 h. This is because the structure of ZIF8 is destroyed under acidic conditions [38].

Antibacterial activity was evaluated by inhibition ring and colony tests of hydrogels against gram-negative (*E. coli*) and gram-positive (*S. aureus*) bacteria. The inhibition rings of the BC/PDA/ZIF8 hydrogel against *E. coli* and *S. aureus* (Supplementary Figure S3, see online supplementary material) verified the antibacterial behavior of BC/PDA/ZIF8–3. To further investigate the antibacterial behavior of the hydrogel, the colony photographs and killing rate are shown in Figure 4c and d, respectively.

Effect of the BC/PDA/ZIF8 hydrogels on cellular proliferation and migration *in vitro*

The cell proliferation for HUVECs and fibroblasts [human foreskin fibroblasts-1 (HFF-1)] in extracts of different hydrogels are shown in Figure 5a, b. The results show that the viability of HUVECs and HFF-1 was supported by all the experimental groups in the first 3 days. However, on day 5, the numbers of proliferating HUVECs and fibroblasts cultured with BC/PDA/ZIF8 hydrogels, especially for the BC/PDA/ZIF8–3 group, was significantly higher than that in BC/PDA hydrogels, indicating that the incorporation of Zn^{2+} stimulates the proliferation of HUVECs and HFF-1.

The results of the qRT–PCR analysis are shown in Figure 5c, d. Figure 5c indicates that compared to the control and BC/PDA hydrogel groups, the expression of FGF was higher in the BC/PDA/ZIF8 hydrogel groups, especially in the BC/PDA/ZIF8–3 group. Figure 5d also shows that the expression of vascular endothelial growth factor (VEGF) was

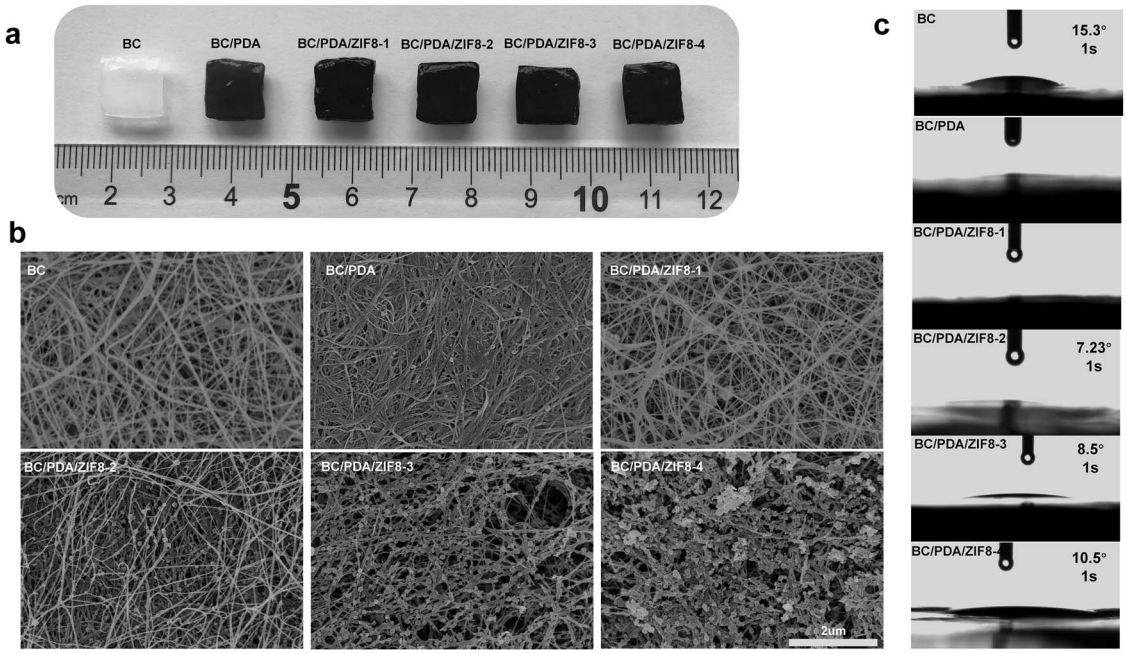

Figure 3. Morphology and hydrophilicity of hydrogels. (**a**) Macrophotographs of BC, BC/PDA, BC/PDA/ZIF8-1, BC/PDA/ZIF8-2, BC/PDA/ZIF8-3, BC/PDA/ZIF8-4 hydrogels. (**b**) FE-SEM micrographs of BC, BC/PDA, BC/PDA/ZIF8-1, BC/PDA/ZIF8-2, BC/PDA/ZIF8-3, BC/PDA/ZIF8-4 hydrogels. (**c**) Contact angles of BC, BC/PDA, BC/PDA/ZIF8-1, BC/PDA/ZIF8-2, BC/PDA/ZIF8-3, BC/PDA/ZIF8-4 hydrogels. *FE-SEM* field emission scanning electron microscope, *BC* bacterial cellulose, *PDA* polydopamine, *ZIF8* zeolitic imidazolate framework 8

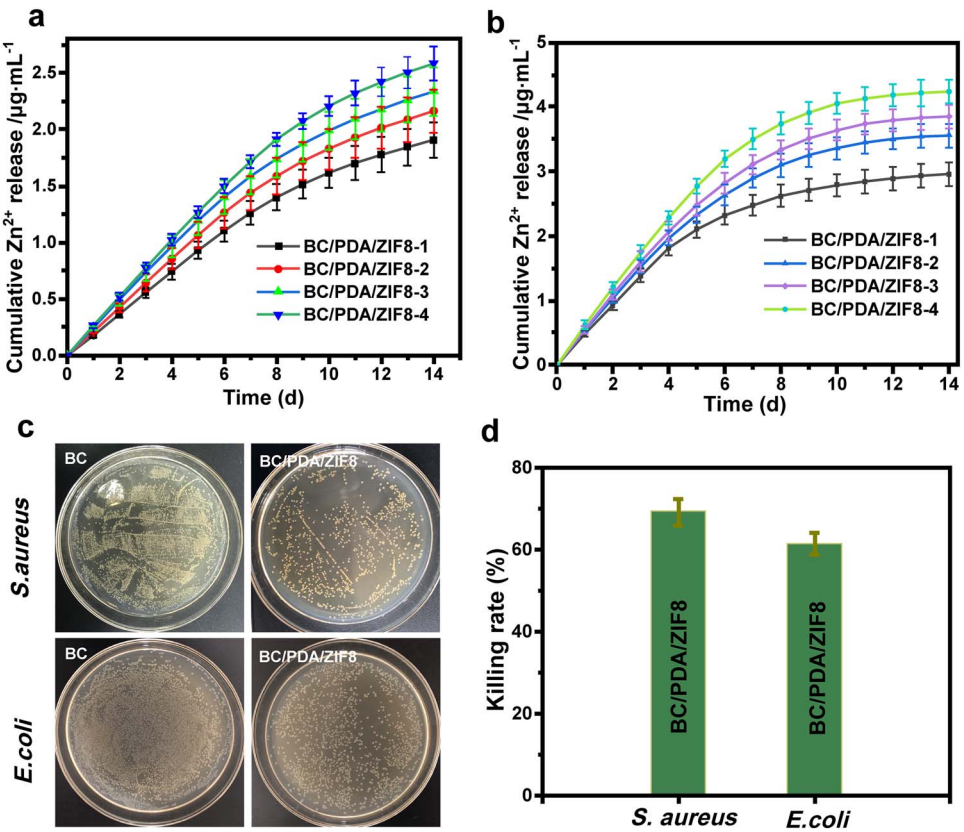

Figure 4. Release behaviors and antibacterial activity of hydrogels. (**a**) Release curve of Zn^{2+} from BC/PDA/ZIF8 hydrogels in PBS at pH = 7.4. (**b**) Release curve of Zn^{2+} from BC/PDA/ZIF8 hydrogels in PBS at pH = 5.5. (**c**) Photographs of colonies of bacteria after treatment with BC/PDA/ZIF8-3 hydrogels. (**d**) Killing rate of BC/PDA/ZIF8-3 hydrogels against *S. aureus* and *E. coli*. *S. aureus* staphylococcus aureus, *E.coli* escherichia coli, *PBS* phosphate-buffered saline, *BC* bacterial cellulose, *PDA* polydopamine, *ZIF8* zeolitic imidazolate framework 8

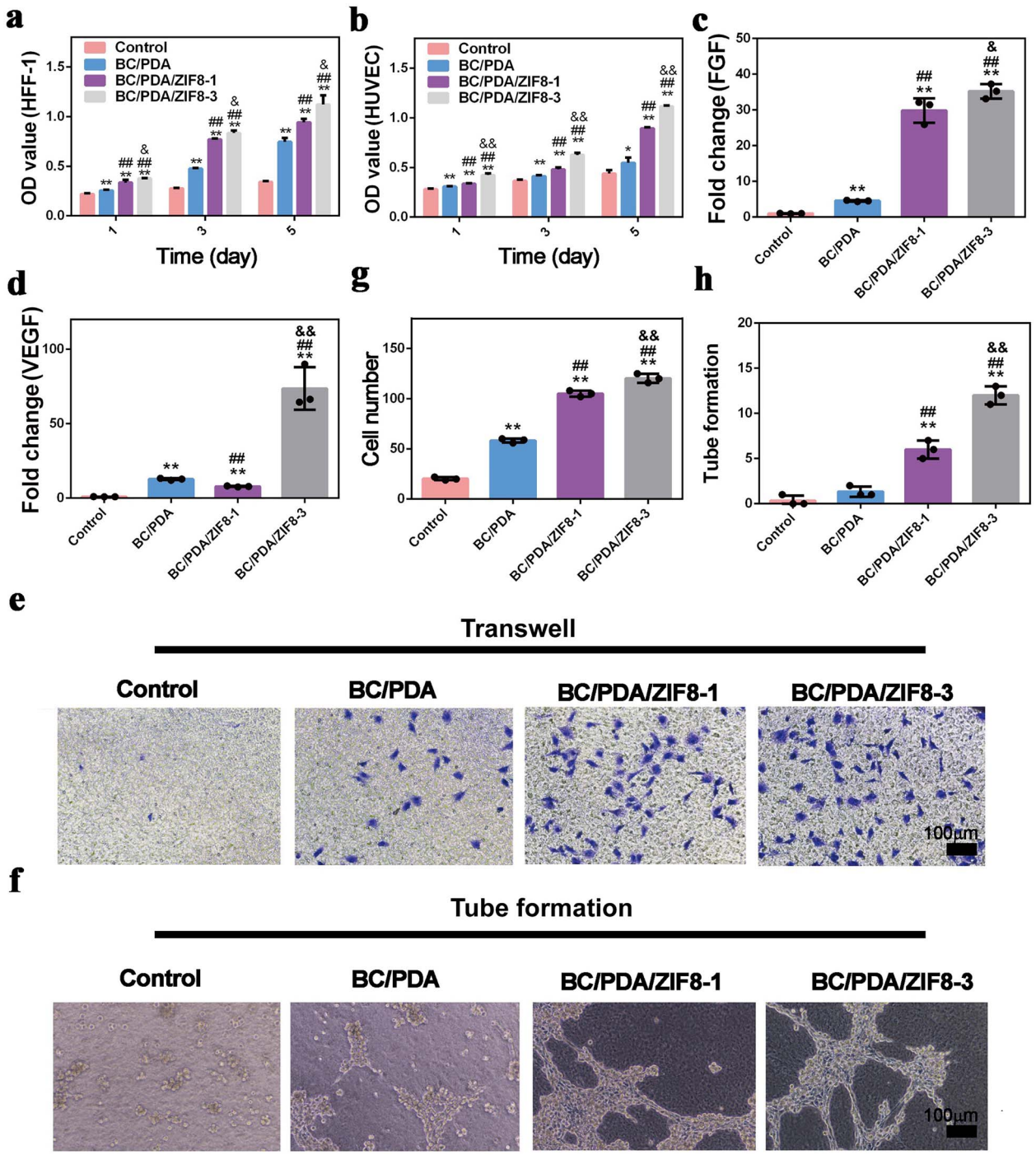

Figure 5. Effect of the BC/PDA/ZIF8 composites on cellular proliferation and migration *in vitro*. (**a**,**b**) Effect of the BC/PDA or BC/PDA/ZIF8 extracts on the proliferation of fibroblasts and HUVECs cultured for 1, 3, and 5 days after immersion in the extracts of the BC/PDA, BC/PDA/ZIF8–1 or BC/PDA/ZIF8–3 hydrogels. (**c**,**d**) Expression levels of fibroblast growth factor (FGF) and VEGF, respectively, in the BC/PDA or BC/PDA/ZIF8 extracts on the fibroblasts and HUVECs. (**e**) Effect of the extract of the BC/PDA and the BC/PDA/ZIF8 hydrogels on the transwell migration(scale bar = 100 μm) of HUVECs after being cultured for 24 h. (**f**) Representative pictures above show the effects of the extracts of the BC/PDA and the BC/PDA/ZIF8 hydrogels on tube formation (scale bar = 100 μm) of HUVECs after being cultured for 6 h. (**g**) Quantitation of HUVEC migration (violet stained cells) using a transwell assay. (**h**) Quantitation of tubule formation by counting the number of complete capillaries connecting individual parts of the polygonal structures. Mean ± SD; n = 6. $^{*}p < 0.05$ compared to the control group; $^{**}p < 0.01$ compared to the control group; $^{\#\#}p < 0.01$ compared to the BC/PDA group; $^{\&}p < 0.05$ compared to the BC/PDA group; $^{\&\&}p < 0.01$ compared to the BC/PDA group. *OD* optical density, *HFF-1* human foreskin fibroblasts-1, *HUVEC* human umbilical vein endothelial cells, *FGF* fibroblast growth factor, *VEGF* vascular endothelial growth factor, *BC* bacterial cellulose, *PDA* polydopamine, *ZIF8* zeolitic imidazolate framework 8

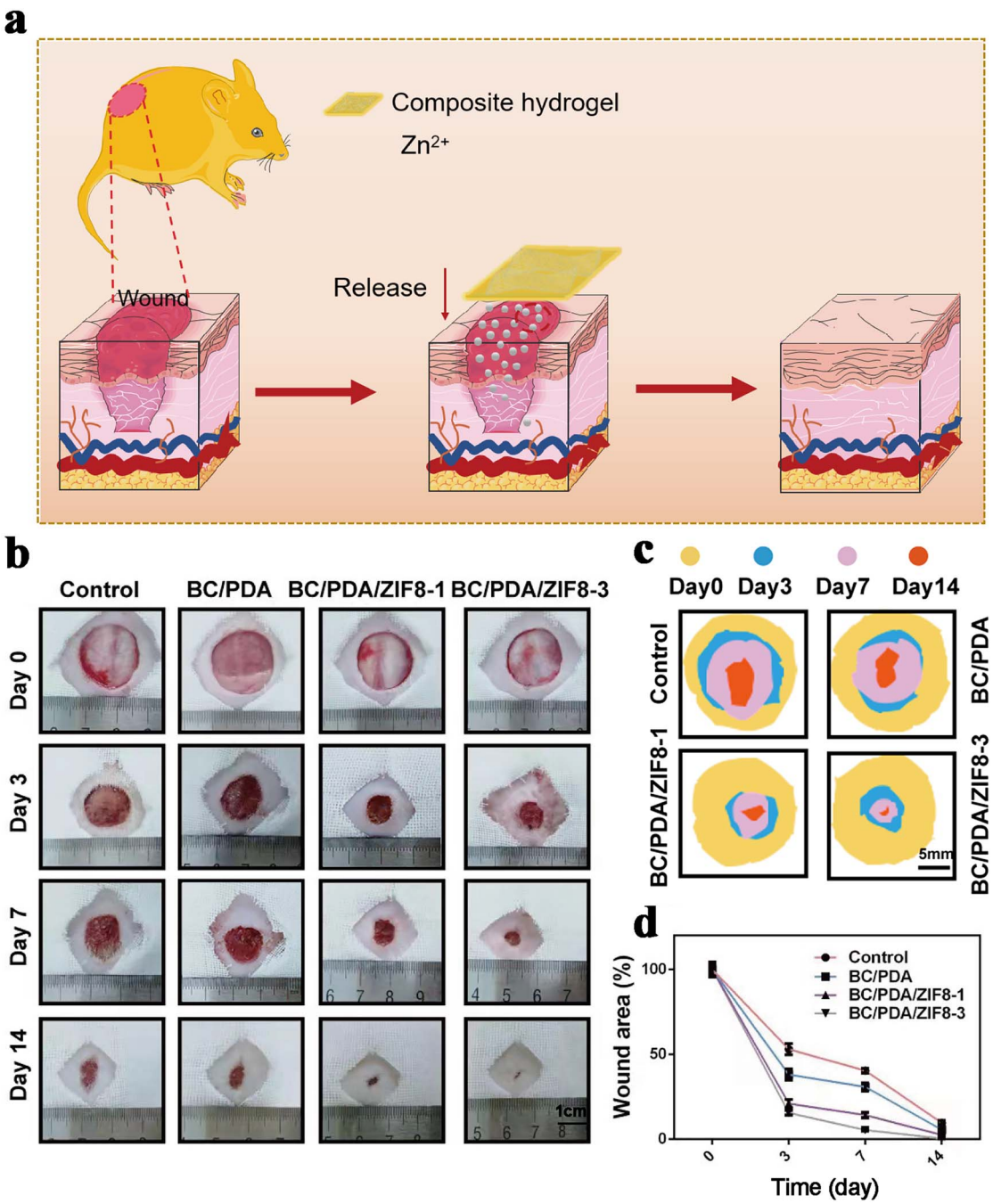

Figure 6. Effect of the BC/PDA/ZIF8 hydrogel on the healing of full-thickness skin defects in rodents. (**a**) Progress of composite hydrogel promoting full-thickness wound healing through releasing Zn^{2+}. (**b**) Representative pictures of full-thickness skin defects in rat models showing treatment with BC/PDA and treatment with BC/PDA/ZIF8–1 or BC/PDA/ZIF8–3 at 3, 7 and 14 days post-surgery (scale bar = 1 cm). (**c**) Traces of wound closure at 3, 7 and 14 days post-surgery (scale bar = 5 mm). (**d**) Wound area (%) for wounds treated with BC/PDA and with BC/PDA/ZIF8–1 or BC/PDA/ZIF8–3 at 3, 7 and 14 days post-surgery. *BC* bacterial cellulose, *PDA* polydopamine, *ZIF8* zeolitic imidazolate framework 8

highest in the BC/PDA/ZIF8–3 group compared with the other groups.

Transwell assays showed the migration behaviors of HUVECs cultured with different hydrogels for 24 h, as shown in Figure 5e, g. The number of migrated HUVECs in the BC/PDA/ZIF8–3 group was higher than that in the BC/PDA group and the BC/PDA/ZIF8–1 group. The BC/PDA/ZIF8–3 group had significantly elevated HUVEC migration of ~70 cells per field and invasion compared with the other groups. The tube formation assay showed that the hydrogels exhibited a significant ability to promote angiogenesis, as shown in Figure 5f, h. When incubated on Matrigel basement for 6 h, HUVECs incubated with BC/PDA/ZIF8 hydrogel extract connected, regulated and formed a network with lumen tubes, especially in the BC/PDA/ZIF8–3 group (40 ± 4/field), but HUVECs in the BC/PDA group produced

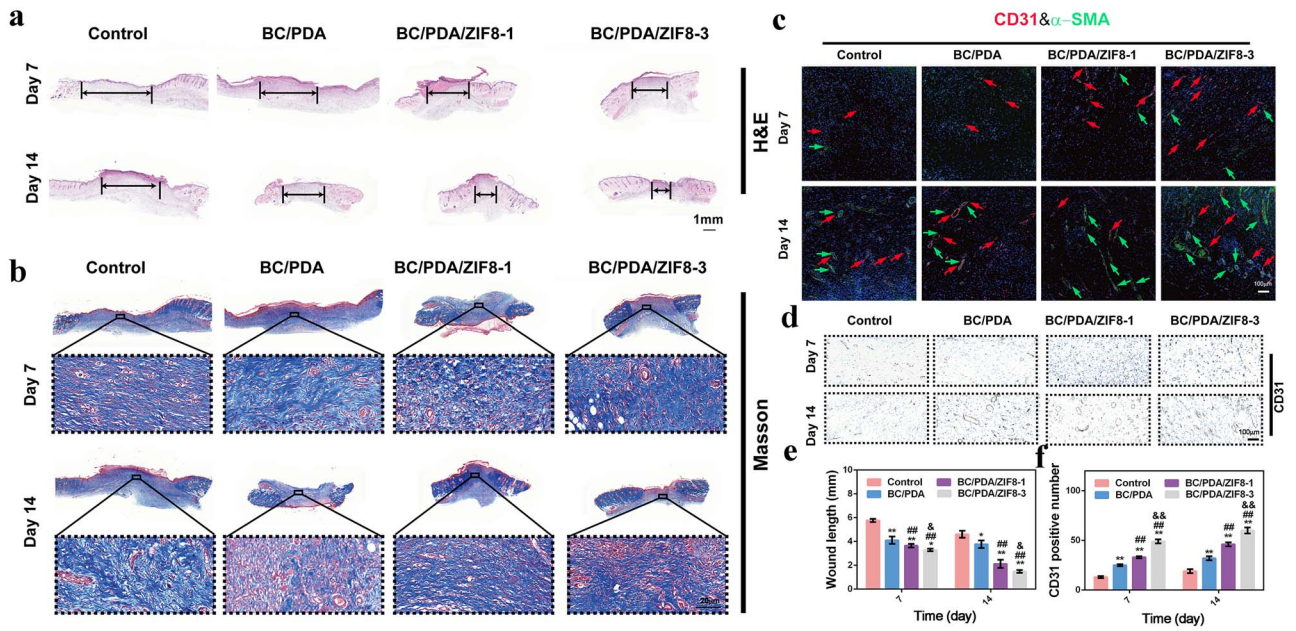

Figure 7. Histological, immunofluorescence and immunohistochemistry assessing angiogenesis and re-epithelialization of hydrogels. (**a**) Transmitted light pictures of H&E-stained parts of the defects treated with BC/PDA and the defects treated with BC/PDA/ZIF8–1 or BC/PDA/ZIF8–3 at 7 and 14 days post-surgery. Scale bar = 1 mm; the total width of the picture represents the initial defect size (2.0 cm) and the markings indicate the neoepithelium. (**b**) Transmitted light pictures of the Masson's trichrome-stained parts of the defects treated with BC/PDA and defects treated with BC/PDA/ZIF8–1 or BC/PDA/ZIF8–3 at 7 and 14 days post-surgery, indicating collagen deposition (scale bar = 20 μm). (**c**) Immunofluorescence staining for endothelial cells (CD31) and alpha-smooth muscle actin (α-SMA) is shown. Endothelial cells (CD31), α-SMA and cell nuclei are stained red, green and blue, respectively. Red and green co-staining represents mature blood vessels (scale bar = 100 μm). (**d**) Immunohistochemistry staining of CD31 in the defects treated with BC/PDA and defects treated with BC/PDA/ZIF8–1 or BC/PDA/ZIF8–3 at 7 and 14 days post-surgery, showing the formation of mature blood vessels (scale bar = 100 μm). (**e**) Wound length in the skin defects treated with BC/PDA and the defects treated with BC/PDA/ZIF8–1 or BC/PDA/ZIF8–3 at 7 and 14 days post-surgery. (**f**) CD31-positive number in the skin defects treated with BC/PDA and the defects treated with BC/PDA/ZIF8–1 or BC/PDA/ZIF8–3 at 7 and 14 days post-surgery. Mean ± SD; $n = 6$. $^{*}p < 0.05$ compared to the control group; $^{**}p < 0.01$ compared to the control group; $^{\#\#}p < 0.01$ compared to the BC/PDA group; $^{\&}p < 0.05$ compared to the BC/PDA/ZIF8-1 group; $^{\&\&}p < 0.01$ compared to the BC/PDA/ZIF8-1 group. *H&E* hematoxylin–eosin, *α-SMA* alpha-smooth muscle actin, *CD31* platelet endothelial cell adhesion molecule-1, *BC* bacterial cellulose, *PDA* polydopamine, *ZIF8* zeolitic imidazolate framework 8

a smaller number of tubes that remained disconnected (Figure 5f).

Effect of the BC/PDA/ZIF8 hydrogels on wound healing in rat models *in vivo*

Full-thickness skin defects were made on the backs of rats and wound healing was observed at 0, 3, 7 and 14 days. No adverse effects were observed in any animals throughout the postoperative period. Figure 6a presents the progress of composite hydrogel promoting full-thickness wound healing through releasing Zn^{2+}. Figure 6b shows digital images of the defects in the control, BC/PDA, BC/PDA/ZIF8–1 and BC/PDA/ZIF8–3 groups at 0, 3, 7 and 14 days. The wound size in the BC/PDA/ZIF8–1 or BC/PDA/ZIF8–3 group was smaller than that in the BC/PDA group (Figure 6c). The wounds treated with BC/PDA/ZIF8–3 were smaller than those treated with BC/PDA/ZIF8–1. The areas of wound closure (Figure 6d) showed that the wounds treated with BC/PDA/ZIF8–3 closed significantly faster than the wounds in the BC/PDA group at three particular time points (days 3, 7 and 14). While the BC/PDA/ZIF8–3 group showed better wound closure than the BC/PDA/ZIF8–1 group, the difference was not significant on day 14.

Histological, immunohistochemistry and immunofluorescence assessment of angiogenesis and re-epithelialization

The re-epithelialization results of H&E staining at 7 and 14 days after surgery showed that in the BC/PDA/ZIF8 group, the length of the new epithelium and the wound closure effect were significantly better than those in the BC/PDA group (Figure 7a, e).

Angiogenesis and fibrogenesis are the basic processes of wound healing. Therefore, we used CD31 immunohistochemistry staining and Masson's trichrome staining to confirm the effect of BC/PDA/ZIF8 hydrogels on wound healing *in vivo*.

Masson's trichrome staining (Figure 7b) showed the difference in collagen deposition and composition between the BC/PDA/ZIF8 and the BC/PDA groups. Compared with the wounds in the BC/PDA group, the BC/PDA/ZIF8–1 group had more collagen deposits and thicker, wavy collagen fibers. However, the BC/PDA/ZIF8–3 group showed more collagen deposition than the BC/PDA/ZIF8–1 group, and the structure of wavy collagen fibers was similar to that of normal skin.

Immunofluorescence staining of CD31 (red) and α-SMA (green) revealed the numbers of mature and newly formed

blood vessels in the different groups (Figure 7c). On the 7th and 14th day, the wounds in the two BC/PDA/ZIF8 groups had higher blood vessel formation density and more mature blood vessels than the wounds of other groups.

The immunohistochemistry staining of CD31 showed the number of mature formed blood vessels in different groups (Figure 7d). Compared with the BC/PDA group, the CD31-positive number in the BC/PDA/ZIF8–1 group was higher, while the BC/PDA/ZIF8–3 group showed a higher CD31-positive number than the BC/PDA/ZIF8–1 group (Figure 7f).

Discussion

The main original finding of this study is that the full-thickness wound healing process is accelerated by BC/PDA/ZIF8 hydrogels. BC/PDA/ZIF8 hydrogels possess antibacterial and angiogenesis abilities proved by *in vitro* and *in vivo* experiments.

BC/PDA/ZIF8 exhibited good tensile strength >1.3 MPa and a modulus of ∼100 kPa. BC/PDA had significantly better mechanical strength than pristine BC, which could be due to the strong hydrogen bonds between BC nanofibers and PDA; in addition, the good adhesion of PDA increases the toughness of the materials. The tensile strength of the BC/PDA/ZIF8 hydrogels was also higher than that of the BC hydrogel, attributed to the enhancement effect of PDA and the restriction of the movement of polymer chains by nanoparticles; however the tensile strength of BC/PDA/ZIF8 was lower than that of BC/PDA, which may be ascribed to ZIF8 nanoparticles disturbing the arrangement of microfibrils, enlarging the distance between BC chains and, to some extent, destroying the hydrogen bonds between nanofibers.

The pure BC hydrogel sample had favorable hydrophilicity with a contact angle of 15.3° due to its plentiful surface –OH, while the BC/PDA sample displayed excellent hydrophilicity with a nonobservable water contact angle, which is the same as the result in a previous report. Although ZIF8 nanoparticles reduced the hydrophilicity of BC, they also exhibited greater hydrophilicity than pristine BC, with a contact angle of 10.5° for BC/PDA/ZIF8–4.

The release behavior of BC/PDA/ZIF8 could be adjusted by controlling the pH and the content of ZIF8. The stable and prolonged release of Zn^{2+} promoted complete wound healing [39]. Compared to the control group, BC/PDA/ZIF8–3 showed good antimicrobial properties with killing rates of 61.6 and 69.3% against *E. coli* and *S. aureus*, respectively. This is attributed to the presence of Zn^{2+}, which can effectively destroy the bacteria [40].

The results of qRT-PCR analysis showed that the incorporation of Zn^{2+} can stimulate the proliferation of HUVECs and fibroblasts by upregulating the expression of VEGF and FGF. The wound healing process involves many links, such as the interaction between ECM, growth factors and various cells. The proliferation of fibroblasts, fibril formation and angiogenesis will eventually shrink the wound area and form epithelium. Endothelial cells (ECs) are the basis of blood vessel formation, and fibroblasts are directly related to the synthesis of ECM proteins and collagen. Among them, the reaction of ECs and fibroblasts is a key factor in wound healing. The initial response of wound healing includes cell proliferation and migration in the wound. Recent studies have shown that Zn^{2+} can effectively stimulate the proliferation and movement of ECs and fibroblasts. In this study, compared with the BC/PDA group, the BC/PDA/ZIF8–3 hydrogel group showed significantly accelerated proliferation of HUVECs and fibroblasts on the third and fifth day (Figure 5a, b). The mechanism by which the endothelial sprouting process promotes angiogenesis is based on EC migration, proliferation and tube formation. The impact on FGF and VEGF expression was also observed in this study, which indicated that the BC/PDA/ZIF8–3 hydrogel group can significantly stimulate the proliferation of HUVECs and fibroblasts (Figure 5c, d). We found that the BC/PDA/ZIF8–3 hydrogel extract significantly enhanced HUVEC migration and tube formation (Figure 5g, h, e, f) to improve the speed of wound healing. Overall, the *in vitro* results of this study indicated that the BC/PDA/ZIF8–3 hydrogel possessed the best performance in promoting tissue regeneration and accelerating the healing of skin wounds by enhancing the vitality of HUVECs and fibroblasts.

The results of *in vivo* experiments showed that the BC/PDA hydrogel could promote wound healing and that BC/PDA/ZIF8–3 achieved faster wound healing than BC/PDA/ZIF8–1. An adequate concentration of Zn^{2+} in the BC/PDA/ZIF8–3 hydrogel might be the reason for the ideal wound healing results.

The neoepithelialization of the wound treated with BC/PDA/ZIF8–3 covered ∼95% of the wound area, and the neoepithelialization of the wound treated with BC/PDA/ZIF8–1 covered ∼90% of the wound area. In the BC/PDA group, wound epithelialization covered only ∼80% of the wound area. Furthermore, in the two BC/PDA/ZIF8 groups, there were significantly more similar structural components of hair follicles and sebaceous glands than in the BC/PDA group. The promotion of re-epithelialization could result from Zn^{2+}-stimulated angiogenesis and fibrogenesis. The results of immunofluorescence and immunohistochemistry staining showed that BC/PDA/ZIF8 groups had higher blood vessel formation density and more mature blood vessels than the wounds of other groups. This phenomenon might be due to the stimulation of mature blood vessel formation by Zn^{2+}.

To achieve a promising translational wound dressing, further research in clinical use is urgently needed. Therefore, a clinical study will be involved in our further research of BC/PDA/ZIF8 hydrogels. It is our goal to make BC/PDA/ZIF8 hydrogels meet actual clinical needs.

Conclusions

This study fabricated a continuous ion delivery system by incorporating Zn^{2+} into a BC hydrogel through autopoly

merization of DA to promote wound healing. This method effectively prevents the agglomeration of nanoparticles and stabilizes the composites for sustained release. Zn^{2+} could stimulate vessel formation and inhibit the growth of *E. coli* and *S. aureus*, while the BC hydrogel was skin-friendly and promoted skin regeneration. The results confirmed that BC/PDA/ZIF8–3 showed the best performance in promoting angiogenesis, collagen formation and epithelial regeneration and exerting antibacterial effects. Meanwhile, the prepared hydrogels could also shield wounds and accelerate wound healing *in vivo*. These results indicate that these BC/PDA/ZIF8 hydrogels are promising translational nanocomposite materials, which may be converted into a new, convenient type of wound dressing with good ease of use and low cost.

Abbreviations

BC: Bacterial cellulose; CFU: Colony forming unit; DA: Dopamine; EC: Endothelial cells ; ECM: Extracellular matrix; FTIR: Fourier transform infrared; H&E: Hematoxylin–eosin; HFF-1: Human foreskin fibroblasts-1; HUVEC: Human umbilical vein endothelial cells; 2-Mim: 2-Methylimidazole; OD: Optical density; PBS: Phosphate-buffered saline; PDA: Polydopamine ; α-SMA: alpha-Smooth muscle actin; UV: Ultraviolet; VEGF: Vascular endothelial growth factor; XRD: X-Ray diffraction; ZIF8: Zeolitic imidazolate framework8.

Authors' contributions

ZH and LD developed the initial concept, designed the experiments and wrote the manuscript. ZH and LD performed the experiments and analyzed the data. YH participated in critically revising the article. SC, HW and YH supervised the study. All authors discussed the results and commented on the manuscript. All authors read and approved the final manuscript.

Acknowledgments

This work was financially supported by the National Natural Science Foundation of China (52003048) and China Postdoctoral Science Foundation (2021 T140110).

Ethics approval

All animal experimental procedures were approved by Shanghai Rat & Mouse Biotech Co.,Ltd [IACUC Issue No. 20220928 (11)].

Supplementary material

Supplementary material is available at *BURNST Journal* online.

Conflict of interest

The authors declare that they have no known competing financial interests or personal relationships that could have appeared to influence the work reported in this paper.

References

1. Armstrong DG, Boulton AJM, Bus SA. Diabetic Foot Ulcers and Their Recurrence. *New England Journal of Medicine New England Journal of Medicine (NEJM/MMS)*. 2017;376:2367–75. Available from: https://www.nejm.org/doi/10.1056/NEJMra1615439.
2. Saleh B, Kaur Dhaliwal H, Portillo-Lara R, Shirzaei Sani E, Abdi R, Amiji MM, *et al*. Local Immunomodulation Using an Adhesive Hydrogel Loaded with miRNA-Laden Nanoparticles Promotes Wound Healing. *Small [Internet] John Wiley & Sons, Ltd*. 2019 [cited 2022 Jan 24];15:1902232. Available from: https://onlinelibrary.wiley.com/doi/full/10.1002/smll.201902232.
3. Jones RE, Foster DS, Longaker MT. Management of Chronic Wounds - 2018. *JAMA - Journal of the American Medical Association American Medical Association*. 2018;320:1481–2. Available from: https://doi.org/10.1001/jama.2018.12426.
4. Zeng R, Lin C, Lin Z, Chen H, Lu W, Lin C, *et al*. Approaches to cutaneous wound healing: basics and future directions. *Cell Tissue Res Springer Verlag*. 2018;374:217–32. Available from: https://doi.org/10.1007/s00441-018-2830-1.
5. Rosenbaum AJ, Banerjee S, Rezak KM, Uhl RL. Advances in wound management. *Journal of the American Academy of Orthopaedic Surgeons Lippincott Williams and Wilkins*. 2018;26:833–43. Available from: https://doi.org/10.5435/JAAOS-D-17-00024.
6. Chen Q, Zhu L, Chen H, Yan H, Huang L, Yang J, *et al*. A novel design strategy for fully physically linked double network hydrogels with tough, fatigue resistant, and self- Healing properties. *Adv Funct Mater Wiley-VCH Verlag*. 2015;25:1598–607. Available from: https://doi.org/10.1002/adfm.201404357.
7. Feng Z, Zuo H, Gao W, Ning N, Tian M, Zhang Feng LZ, *et al*. A Robust, Self-Healable, and Shape Memory Supramolecular Hydrogel by Multiple Hydrogen Bonding Interactions. *Macromol Rapid Commun [Internet] John Wiley & Sons, Ltd*. 2018 [cited 2022 Jan 24];39:1800138. Available from: https://onlinelibrary.wiley.com/doi/full/10.1002/marc.201800138.
8. Zheng L, Li S, Luo J, Wang X. Latest Advances on Bacterial Cellulose-Based Antibacterial Materials as Wound Dressings. *Front Bioeng Biotechnol Frontiers Media SA*. 2020;8. Available from: https://doi.org/10.3389/fbioe.2020.593768.
9. Luo Z, Liu J, Lin H, Ren X, Tian H, Liang Y, *et al*. In situ fabrication of nano zno/bcm biocomposite based on ma modified bacterial cellulose membrane for antibacterial and wound healing. *Int J Nanomedicine Dove Medical Press Ltd*. 2020;15:1–15. Available from: https://doi.org/10.2147/IJN.S231556.
10. Daria Ciecholewska-Juśko, Anna Żywicka, Adam Junka, Radosław Drozd, Peter Sobolewski, Paweł Migdał, *et al*. Superabsorbent crosslinked bacterial cellulose biomaterials for chronic wound dressings. *Carbohydrate Polymers (IF 10.723)*. 2020. https://doi.org/10.1016/j.carbpol.2020.117247.
11. Wang YJ, Li CY, Wang ZJ, Zhao Y, Chen L, Wu ZL, *et al*. Hydrogen bond-reinforced double-network hydrogels with ultrahigh elastic modulus and shape memory property. *J Polym Sci B Polym Phys John Wiley and Sons Inc*. 2018;56:1281–6. Available from: https://doi.org/10.1002/polb.24620.
12. Yang J, Cristian V, Dong A, Zhang J. A Facile Strategy to Achieve Synergistic Multiple Hydrogen Bonding Interactions for Constructing Robust Hydrogels with Self-healing Capability, Shape Transformation and Actuation Function. *Macromol Chem Phys John Wiley and Sons Inc*. 2021;222. Available from: https://doi.org/10.1002/macp.202000429.

13. Ciecholewska-Juśko D, Żywicka A, Junka A, Drozd R, Sobolewski P, Migdał P, *et al.* Superabsorbent crosslinked bacterial cellulose biomaterials for chronic wound dressings. *Carbohydr Polym Elsevier Ltd*. 2021;253. Available from: https://doi.org/10.1016/j.carbpol.2020.117247.
14. Wu Z, Chen S, Wu R, Sheng N, Zhang M, Ji P, *et al.* Top-down peeling bacterial cellulose to high strength ultrathin films and multifunctional fibers. *Chemical Engineering Journal Elsevier BV*. 2020;391. Available from: https://doi.org/10.1016/j.cej.2019.123527.
15. Peng Y, He D, Ge X, Lu Y, Chai Y, Zhang Y, *et al.* Construction of heparin-based hydrogel incorporated with Cu5.4O ultrasmall nanozymes for wound healing and inflammation inhibition. *Bioact Mater Elsevier*. 2021;6:3109–24. Available from: https://doi.org/10.1016/j.bioactmat.2021.02.006.
16. Liao M, Wan P, Wen J, Gong M, Wu X, Wang Y, *et al.* Wearable, Healable, and Adhesive Epidermal Sensors Assembled from Mussel-Inspired Conductive Hybrid Hydrogel Framework. *Adv Funct Mater Wiley-VCH Verlag*. 2017;27. Available from: https://doi.org/10.1002/adfm.201703852.
17. Rong Q, Lei W, Chen L, Yin Y, Zhou J, Liu M. Anti-freezing, Conductive Self-healing Organohydrogels with Stable Strain-Sensitivity at Subzero Temperatures. *Angewandte Chemie - International Edition Wiley-VCH Verlag*. 2017;56:14159–63. Available from: https://doi.org/10.1002/anie.201708614.
18. Li A, Han Z, Li Z, Li J, Li X, Zhang Z. A PTHrP-2 loaded adhesive cellulose acetate nanofiber mat as wound dressing accelerates wound healing. *Mater Des Elsevier*. 2021;212: 110241. Available from: https://doi.org/10.1016/j.matdes.2021.110241.
19. Ardekani NT, Khorram M, Zomorodian K, Yazdanpanah S, Veisi H, Veisi H. Evaluation of electrospun poly (vinyl alcohol)-based nanofiber mats incorporated with Zataria multiflora essential oil as potential wound dressing. *Int J Biol Macromol Elsevier BV*. 2019;125:743–50. Available from: https://doi.org/10.1016/j.ijbiomac.2018.12.085.
20. Adeli H, Khorasani MT, Parvazinia M. Wound dressing based on electrospun PVA/chitosan/starch nanofibrous mats: Fabrication, antibacterial and cytocompatibility evaluation and in vitro healing assay. *Int J Biol Macromol Elsevier BV*. 2019;122:238–54. Available from: https://doi.org/10.1016/j.ijbiomac.2018.10.115.
21. Ullah A, Ullah S, Khan MQ, Hashmi M, Nam PD, Kato Y, *et al.* Manuka honey incorporated cellulose acetate nanofibrous mats: Fabrication and in vitro evaluation as a potential wound dressing. *Int J Biol Macromol Elsevier*. 2020;155:479–89. Available from: https://doi.org/10.1016/j.ijbiomac.2020.03.237.
22. Banno K, Yoder MC. Tissue regeneration using endothelial colony-forming cells: promising cells for vascular repair. *Pediatr Res Nature Publishing Group*. 2018;83:283–90. Available from: https://doi.org/10.1038/pr.2017.231.
23. McDonald AI, Shirali AS, Aragón R, Ma F, Hernandez G, Vaughn DA, *et al.* Endothelial regeneration of large vessels is a biphasic process driven by local cells with distinct proliferative capacities. *Cell Stem Cell Cell Press*. 2018;23:210, e216. Available from:–25. https://doi.org/10.1016/j.stem.2018.07.011.
24. Liu H, Li Z, Zhao Y, Feng Y, Zvyagin AV, Wang J, *et al.* Novel Diabetic Foot Wound Dressing Based on Multifunctional Hydrogels with Extensive Temperature-Tolerant, Durable, Adhesive, and Intrinsic Antibacterial Properties. *ACS Appl Mater Interfaces American Chemical Society*. 2021;13:26770–81. Available from: https://doi.org/10.1021/acsami.1c05514.
25. Huang J, Lin D, Wei Z, Li Q, Zheng J, Zheng Q, *et al.* Parathyroid Hormone Derivative with Reduced Osteoclastic Activity Promoted Bone Regeneration via Synergistic Bone Remodeling and Angiogenesis. *Small Wiley-VCH Verlag*. 2020;16. Available from: https://doi.org/10.1002/smll.201905876.
26. Mi B, Chen L, Xiong Y, Yang Y, Panayi AC, Xue H, *et al.* Osteoblast/Osteoclast and Immune Cocktail Therapy of an Exosome/Drug Delivery Multifunctional Hydrogel Accelerates Fracture Repair. *ACS Nano [Internet] American Chemical Society*. 2022 [cited 2022 Apr 1];16:771–82. Available from: https://pubs.acs.org/doi/full/10.1021/acsnano.1c08284.
27. Götz W, Reichert C, Canullo L, Jäger A, Heinemann F. Coupling of osteogenesis and angiogenesis in bone substitute healing - A brief overview. *Ann Anat*. 2012;194:171–3. Available from: https://doi.org/10.1016/j.aanat.2011.10.002.
28. Karimi A, Khataee A, Vatanpour V, Safarpour M. High-flux PVDF mixed matrix membranes embedded with size-controlled ZIF-8 nanoparticles. *Sep Purif Technol Elsevier BV*. 2019;229. Available from: https://doi.org/10.1016/j.seppur.2019.115838.
29. Mao L, Wang L, Zhang M, Ullah MW, Liu L, Zhao W, *et al.* In Situ Synthesized Selenium Nanoparticles-Decorated Bacterial Cellulose/Gelatin Hydrogel with Enhanced Antibacterial, Antioxidant, and Anti-Inflammatory Capabilities for Facilitating Skin Wound Healing. *Adv Healthc Mater John Wiley and Sons Inc*. 2021;10. Available from: https://doi.org/10.1002/adhm.202100402.
30. Zhai R, Chen X, Jin M, Hu J. Synthesis of a polydopamaine nanoparticle/bacterial cellulose composite for use as a biocompatible matrix for laccase immobilization. *Cellulose Springer Netherlands*. 2019;26:8337–49. Available from: https://doi.org/10.1007/s10570-019-02588-6.
31. Zhang M, Shang Q, Wan Y, Cheng Q, Liao G, Pan Z. Self-template synthesis of double-shell TiO2@ZIF-8 hollow nanospheres via sonocrystallization with enhanced photocatalytic activities in hydrogen generation. *Appl Catal B Elsevier BV*. 2019;241:149–58. Available from: https://doi.org/10.1016/j.apcatb.2018.09.036.
32. Fan Z, Liu B, Wang J, Zhang S, Lin Q, Gong P, *et al.* A novel wound dressing based on Ag/graphene polymer hydrogel: Effectively kill bacteria and accelerate wound healing. *Adv Funct Mater Wiley-VCH Verlag*. 2014;24:3933–43. Available from: https://doi.org/10.1002/adfm.201304202.
33. Li Y, Tian Y, Zheng W, Feng Y, Huang R, Shao J, *et al.* Composites of Bacterial Cellulose and Small Molecule-Decorated Gold Nanoparticles for Treating Gram-Negative Bacteria-Infected Wounds. *Small [Internet] John Wiley & Sons, Ltd*. 2017 [cited 2022 Apr 26];13:1700130. Available from: https://onlinelibrary.wiley.com/doi/full/10.1002/smll.201700130.
34. Lai C, Zhang SJ, Sheng LY, Xi TF. Comparative evaluation of the biocompatible and physical-chemical properties of poly(lactide-co-glycolide) and polydopamine as coating materials for bacterial cellulose. *J Mater Chem B Royal Society of Chemistry*. 2019;7:630–9. Available from: https://doi.org/10.1039/C8TB02456A.
35. Wang B, Lv X, Li Z, Zhang M, Yao J, Sheng N, *et al.* Urethra-inspired biomimetic scaffold: A therapeutic strategy to promote angiogenesis for urethral regeneration in a rabbit model. *Acta Biomater Acta Materialia Inc*. 2020;102:247–58. Available from: https://doi.org/10.1016/j.actbio.2019.11.026.

36. Yang L, Chen C, Hu Y, Wei F, Cui J, Zhao Y, *et al*. Three-dimensional bacterial cellulose/polydopamine/TiO2 nanocomposite membrane with enhanced adsorption and photocatalytic degradation for dyes under ultraviolet-visible irradiation. *J Colloid Interface Sci Academic Press*. 2020;562:21–8. Available from: https://doi.org/10.1016/j.jcis.2019.12.013.
37. Inoue Y, Hasegawa S, Ban S, Yamada T, Date Y, Mizutani H, *et al*. ZIP2 protein, a zinc transporter, is associated with keratinocyte differentiation. Journal of Bio logical Chemistry. *American Society for Biochemistry and Molecular Biology Inc*. 2014;289:21451–62. Available from: https://doi.org/10.1074/jbc.M114.560821.
38. Xiao J, Zhou Y, Ye M, An Y, Wang K, Wu Q, *et al*. Freeze-Thawing Chitosan/Ions Hydrogel Coated Gauzes Releasing Multiple Metal Ions on Demand for Improved Infected Wound Healing. *Adv Healthc Mater John Wiley and Sons Inc*. 2021;10. Available from: https://doi.org/10.1002/adhm.202001591.
39. Wang Y, Ying T, Li J, Xu Y, Wang R, Ke Q, *et al*. Hierarchical micro/nanofibrous scaffolds incorporated with curcumin and zinc ion eutectic metal organic frameworks for enhanced diabetic wound healing via anti-oxidant and anti-inflammatory activities. *Chemical Engineering Journal Elsevier BV*. 2020;402. Available from: https://doi.org/10.1016/j.cej.2020.126273.
40. Zhang M, Chen S, Zhong L, Wang B, Wang H, Hong F. Zn2+−loaded TOBC nanofiber-reinforced biomimetic calcium alginate hydrogel for antibacterial wound dressing[J]. *Int J Biol Macromol*. 2020;143:235–42. Available from: https://doi.org/10.1016/j.ijbiomac.2019.12.046.